



HAL
open science

Effect of ballistic damage in UO₂ samples under ion beam irradiations studied by in situ Raman spectroscopy

G. Gutierrez, Claire Onofri, S. Miro, M. Bricout, F. Leprêtre

► **To cite this version:**

G. Gutierrez, Claire Onofri, S. Miro, M. Bricout, F. Leprêtre. Effect of ballistic damage in UO₂ samples under ion beam irradiations studied by in situ Raman spectroscopy. Nuclear Instruments and Methods in Physics Research Section B: Beam Interactions with Materials and Atoms, 2018, 434, pp.45-50. 10.1016/j.nimb.2018.08.010 . cea-02339665

HAL Id: cea-02339665

<https://cea.hal.science/cea-02339665v1>

Submitted on 4 Nov 2019

HAL is a multi-disciplinary open access archive for the deposit and dissemination of scientific research documents, whether they are published or not. The documents may come from teaching and research institutions in France or abroad, or from public or private research centers.

L'archive ouverte pluridisciplinaire **HAL**, est destinée au dépôt et à la diffusion de documents scientifiques de niveau recherche, publiés ou non, émanant des établissements d'enseignement et de recherche français ou étrangers, des laboratoires publics ou privés.

Effect of ballistic damage in UO_2 samples under ion beam irradiations studied by *in situ* Raman spectroscopy

G. Gutierrez^{1*}, C. Onofri², S. Miro¹, M. Bricout¹, F. Leprêtre¹

¹DEN-Service de Recherches de Métallurgie Physique, CEA, Paris-Saclay Univ., F-91191 Gif-sur-Yvette, France

²CEA, DEN, DEC, F-13108 St Paul lez Durance, France.

* corresponding author: gaelle.gutierrez@cea.fr

Abstract

The damage induced in uranium dioxide (UO_2) during ion irradiation at low energy was studied by micro-Raman spectroscopy. Polycrystalline UO_2 samples were irradiated by 0.9-MeV I, 2-MeV Au at 25°C and by 4-MeV Kr ions at -160°C in a wide range of fluence. In situ Raman measurements reveal similar spectra evolution no matter the ion beam used. The T_{2g} band centred at 445 cm^{-1} related to the fluorine structure reveals a broadening with the irradiation damage increase. In addition, several bands ranging from 500 to 700 cm^{-1} , which are attributed to sub- or sur-stoichiometric structural defects, are observed at the first time of irradiation. Their intensities rise up with the irradiation fluence increase to a similar asymptotic relative values for all the irradiation conditions. The obtained Raman kinetics are compared with data from the literature on the microstructure evolution observed by Transmission Electronic Microscopy (TEM) and on the fraction of displaced atoms determined by Rutherford Backscattering Spectroscopy in channelling mode (RBS-C).

Intro

Raman spectroscopy is an efficient technique to determine the structural evolution in materials under irradiation. Nuclear fuel [1], cladding materials [2] or matrices for high level nuclear waste management [3] have been successfully characterized by this technique. Radioactive fuel samples [4, 5] as well as ion beam irradiated uranium dioxide (UO₂) samples [6,7] can be studied and compared. Several papers have investigated the Raman spectra evolution of UO₂ after ion beam irradiation [1, 6, 7]. In addition to the standard T_{2g} band, additional bands in the range of 500 to 700 cm⁻¹ are observed after sample oxidation or are induced by ion irradiation performed under vacuum [1, 4-7]. At 575 cm⁻¹, the LO Raman-forbidden mode in the perfect fluorite structure becomes active by the presence of disorder in the crystal due to a breakdown in the selection rules [1, 8]. Two other bands at around 520 and 630 cm⁻¹ denoted as U1 and U3 could be associated with sub-stoichiometry UO_{2-x} and with structural defects in the cuboctahedral symmetry of the interstitial oxygen in hyper-stoichiometric UO₂, respectively [7, 9, 10].

The present study aims to investigate the effect of ballistic damage generated by ion beam irradiations in UO₂. The damage kinetics of polycrystalline samples under ion beam irradiation was monitored in real time by using the JANNuS (Joint Accelerators for Nanoscience and Nuclear Simulation) platform in Saclay, France. *In situ* Raman setup with a frequency-doubled Nd: YAG (532 nm) laser is coupled with a triple beam chamber [11]. Samples were irradiated with low energy ions in order to determine the Raman spectra evolution under ballistic damage. Experiments have been performed at room temperature (25°C) with I ions at an energy of 0.9 MeV and with Au ions at 2 MeV. A complementary irradiation at low temperature (-160°C) has been also carried out with Kr ions at an energy of 4 MeV. To follow in real time the radiation damage evolution, *in situ* Raman spectra have been recorded for different irradiation fluences.

Experimental procedures

UO₂ polycrystalline pellets with an average grain size of 7.6 μm were cut in discs (thickness: 500 μm) and polished on one side. An annealing at 1400°C during 4 h under an Ar-H₂ (5%) was performed in order to remove the damage induced by polishing. Pellet density has been measured to be around 10.74 g.cm⁻³ (~98 % of densification).

The irradiations were carried out at JANNuS-Saclay facility with 0.9 MeV I ions and 2 MeV Au ions at a controlled temperature of 25°C and with 4 MeV Kr ions at -160°C. The irradiations were performed

under a vacuum lower than 10^{-7} mbar in order to prevent any oxidation. Irradiation conditions and parameters calculated using the SRIM code are reported in Tab.1 [12].

The JANNuS facility also includes the possibility of *in situ* Raman monitoring during irradiation. The experimental set up is described in [11]. Raman spectra were recorded in broad wave-number range between 200 and 900 cm^{-1} for virgin and irradiated samples using an Invia Reflex Renishaw spectrometer coupled with a Leica microscope. A laser power lower than 1 mW was used in order to avoid oxidation during the analysis. *In situ* Raman measurements after beam shut off were carried on irradiated samples with a frequency-doubled Nd:YAG (532 nm) laser and a 2400 groove/mm grating. The Raman spectrometer has been calibrated by using silicon monocrystalline samples. Raman spectra were recorded during 120 s at each step of irradiation fluence. Raman spectrum can be recorded during ion irradiation but, in order to obtain representative data avoiding any additional evolution of the microstructure, the ion beam is stopped during the acquisitions.

The fitting module of the Wire Raman spectroscopy software (Renishaw) was used for the spectra simulation. A combination of Lorentzian (often used for crystal) and Gaussian line shape (expected for disordered materials) called Voigt profiles was used. The accuracy on band position deduced from spectrum simulation is determined at $\pm 1 \text{ cm}^{-1}$.

Results

The figure 1 presents the Raman spectra between 300 and 900 cm^{-1} *in situ* recorded on UO_2 samples irradiated with 2 MeV Au ions at 25°C for fluences ranging from 4.7×10^{12} to $1.2 \times 10^{16} \text{ Au.cm}^{-2}$. Before irradiation (spectrum 0 in black), we observed a band centred at 445 cm^{-1} assigned to the triply degenerate Raman active mode (T_{2g}) commonly Raman active for all the fluorine structures [14]. This band is related to the breathing vibration of oxygen atoms around the uranium atoms in the crystalline structure. In the 500 and 700 cm^{-1} range, we also remark one intense band at 575 cm^{-1} and two bands with a smaller intensity at 520 and 630 cm^{-1} . The band at 575 cm^{-1} is associated to the first order T_{1u} LO scattering mode [8]. This mode is Raman-forbidden in the perfect fluorite structure and becomes active by the presence of disorder in the crystal due to a breakdown in the selection rules [1, 8]. The assignment of 520 and 630 cm^{-1} bands is less obvious. The first one denoted as U1 is associated with sub-stoichiometry UO_{2-x} [1]. The third band denoted U3 is assigned to structural defects in the cuboctahedral symmetry of the interstitial oxygen in hyper-stoichiometric UO_2 [7]. This triplet band (U1,

LO, U3) is already observable before irradiation highlighting the presence of defect in the virgin samples due to the preparation or to a surface oxidation [15]. As shown on Fig.1, from our first fluence ($4.7 \times 10^{12} \text{ Au.cm}^{-2}$) to $10^{14} \text{ Au.cm}^{-2}$, the intensity of T_{2g} band decreases and a broadening is observed. In addition, the triplet bands in the range of $500\text{-}700 \text{ cm}^{-1}$ increases. The U1 and U3 bands less marked on the virgin samples are more intense after irradiation. Then, from an irradiation fluence of $10^{14} \text{ Au.cm}^{-2}$, the Raman spectra do not seem to evolve any more. We must note that our Raman measurements have been performed with a 532 nm wavelength laser. In these analysis conditions, the LO band is much more intense compared to the U1 and U3 bands due to a resonance effect [16]. The U1 and U3 evolutions is more difficult to follow especially for low damage level. For that reason, in the following part, the triplet band in the 500 and 700 cm^{-1} range will be discussed together and referred as the defect massif.

The Raman spectra have also been *in situ* recorded for UO_2 samples irradiated at 25°C with 0.9 MeV I ions and at -160°C with 4 MeV Kr ions. We observed a similar evolution with an increase of the defect massif area at first step of irradiation and a decrease of T_{2g} band with a broadening. In order to compare the results obtained from the different irradiations, the line width (FWHM) of T_{2g} band, characteristic to the undisturbed fluorite lattice, is reported on Fig. 2.a as a function of the maximum displacement per atoms (dpa). It exhibits similar evolution for all the irradiated samples. Below 0.03 dpa, no significant linewidth evolution is observed. After an irradiation inducing 0.03 dpa, a broadening occurs and increases linearly with the damage. Then a stabilization at an asymptotic relative value of around 30 cm^{-1} is shown. In addition, a small T_{2g} shift ($<1.5 \text{ cm}^{-1}$) to the lower frequencies is noticed for all the irradiations.

Since the defect massif is associated to the structural disorder, the ratio between its area and T_{2g} band area describes the damage build-up kinetics in UO_2 for different irradiation conditions. Fig. 2.b presents this ratio as a function of the maximum dpa. We observed that, as soon as the UO_2 samples are submitted to irradiation damage (first step at 0.001 dpa), the band intensity increase for all the curves. We notice a shift of massif defect evolution between the samples irradiated at 25°C and the one at -160°C . It indicates that the area increase occurs in a faster way for the irradiation performed at low temperature (Kr) than for the ones at room temperature (I, Au). A similar asymptotic relative value is achieved for all the irradiation conditions but at different damage level according to the irradiation temperature. The evolution of defect massif area is well reproduced by the multiple step damage

accumulation (MSDA) model [17]. The evolutions inducing during I ions irradiation at 25°C and Kr ions irradiation at -160°C have been fitted by the following equation (Fig. 3):

$$f_D = \sum_{i=1}^{n-1} \left\{ f_{D,i}^{\text{sat}} G [1 - \exp(-\sigma_i(\Phi - \Phi_i))] \prod_{k=1}^n [\exp(-\sigma_{k+1}(\Phi - \Phi_{k+1}))] \right\} + f_{D,n}^{\text{sat}} G [1 - \exp(-\sigma_n(\Phi - \Phi_n))] \quad (1)$$

where $f_{D,i}^{\text{sat}}$ is the level of damage at saturation, n is the number of steps required for the achievement of the total disordering process, Φ_i is the threshold ion fluence of the i^{th} step, and σ_i the disordering cross-section at the i^{th} step. G corresponds to the Heaviside function H multiplied by its argument. In the MSDA model, the damage accumulation results from atomic rearrangements steps induced by microscopic and/or macroscopic events [17]. Each step is correlated to a new defect configuration, which is generated by the damage accumulation. In our case, the damage build-up is accumulated via a two-step mechanism ($n = 2$ in Eq. (1)): the first step up to 0.065 and 0.0054 dpa at an irradiation temperature of 25°C and -160°C, respectively, and the second for higher value. The first step occurs for a very small amount of damage level and is shorter for the lower irradiation temperature. Concerning the second step, it is interesting to note that a higher disordering cross-section (σ_2) is determined for an irradiation at a temperature of -160°C (12.7 nm²) than at 25°C (3.7 nm²). These results indicate a faster increase of level damage for an irradiation temperature of -160°C. The level of damage at saturation ($f_{D,2}^{\text{sat}}$) decreases from 5.3 at 25°C down to 4.8 at -160°C. However, due to our resolution limit, this difference is not quite significant. Thus, the first step observed for very low damage level, should be, for example, the consequence of point defect evolving in clusters on the Raman spectra. However, complementary experiments are required to conclude on this point.

Discussion

The results from the different irradiation experiments highlight that, during an irradiation favouring the ballistic damage at 25°C, one damage level (dpa) seems to induce one Raman spectra. Indeed, we have observed that a broadening and an intensity decrease of T_{2g} band occur for all the performed irradiations. The intensity loss of the T_{2g} band indicates deviations from the perfect cubic fluorite structure [9]. In addition, the disorder arising from irradiation induces the relaxation of selection rules allowing a greater range of vibrational modes to contribute to Raman scattering. This could be experimentally observed by an asymmetrical broadening of the Raman band [18, 19]. We do also measure a shift to lower frequencies with a value closed to our resolution limit (<1.5 μm). Similar T_{2g} red-shift was reported for UO₂ samples irradiated with He²⁺ at 25 MeV and in self-irradiated samples

[7, 5]. It could highlight the defects formation (point defects, dislocations or voids) and a lattice swelling. This point will be discussed in the following part by comparing the evolution kinetics of different defects obtained by other characterizations (TEM and RBS-C).

In addition, the defect massif area, correlated with the damage build-up, increases with the irradiation doses and then reaches saturation at the dose of around 0.2-0.4 dpa (Fig. 2). The cross section analysis of an irradiated samples with He ions at 25 MeV by Raman spectroscopy highlights also a T_{2g} broadening correlated with a grow up of U1, LO and U3 bands area when the ballistic stopping power becomes predominant compared to the electronic one [7]. The Raman spectra comparison between the irradiations performed at 25°C and -160°C indicates a faster increase of level damage for an irradiation at -160°C. It could be explained by the freezing of generated defects at low temperature and a higher recombination during the irradiation at 25°C [20]. However, a stabilization at a closed asymptotic value of T_{2g} linewidth and defect massif area were observed. This increase of defect massif was also reported in literature after irradiations with Kr ions at an energy of 0.2 MeV [6] and of 4 MeV [21].

Indeed, after an irradiation at 500°C with Kr ions at an energy of 4 MeV, Onofri *et al.* reported an increase of defect massif area up to 6 times higher than for the virgin one after an irradiation fluence of 3.10^{16} Kr.cm⁻² (i.e. 90 dpa) then a saturation is reached for higher fluences [21]. This ratio difference is closed to the one obtained in our study (around 5 times compared to the virgin samples). It seems to show that no matter the irradiation temperature the area ratio between defect massif and T_{2g} band stabilizes at a quite similar value indicating a similar measured disordered level or saturation of Raman signal. However, as no Raman measurement has been performed at lower Kr irradiation fluence by [21], we cannot conclude if this saturation is achieved for a higher damage level at a higher irradiation temperature.

Point defects generated by irradiation can cluster forming extended defects such as voids and dislocation loops. Several studies report the nucleation of dislocations loops at very low damage level [22-26]. For instance, Onofri *et al.* have *in situ* observed the first dislocation loops nucleation under irradiation at -180°C with 0.39 MeV Xe ions from a damage level of around 0.008 dpa [25] (Fig. 4.a). The loop density increases with the irradiation fluence up to a saturation value, which depends on the temperature [22, 23, 25]. Then, a decrease occurs due to the formation of dislocation line. Lastly, the loop density remains constant. Thus, the evolution kinetics of dislocations is very different from the

one observed in the current work (Fig. 4.a). Simultaneously to the dislocation formation, voids nucleation was observed at low damage level too [27-29]. The bubble/cavity density increases in the first time of the irradiation and then reaches a constant value of $2 - 4 \times 10^{24} \text{ m}^{-3}$. The voids generated in UO_2 samples under irradiation with Au ions at 4 MeV at 25°C and observed *in situ* by Sabathier *et al.* [27] were compared to our Raman spectra change. Fig. 4.b gathers the value of defect massif area during the 0.9 MeV I ions irradiation at 25°C and the void density as a function of the generated dpa. Quite similar evolution is shown by the both techniques. The first voids observation is noticed at low damage level (0.03 dpa) which is correlated with the increase of massif defect area at our first irradiation step (0.001 dpa). Then, no significant evolution of the defect massif or of the void density was observed after an irradiation inducing around 0.3 dpa.

Lastly, Rutherford Backscattering Spectroscopy in Channelling mode (RBS-C) can characterize the fraction of displacement atoms (f_D) during irradiation. Fig. 5 presents the damage kinetics obtained by RBS-C during 0.5 MeV La ions irradiation at 25°C as function as the maximum dpa [30]. The damage fraction increase occurs for values higher than 4 dpa whereas the value of defect massif area during the 0.9 MeV I ions increases after a radiation damage of 0.03 dpa. It clearly indicates that the two evolutions are not similar. However, for UO_2 samples, ion channelling is able to measure disorder on the U sub-lattice and O sub-lattice but with different cross section. Indeed, by using the $^{16}\text{O}(^4\text{He}, ^4\text{He})^{16}\text{O}$ resonant reaction with He ions at an energy of 3.085 MeV, the backscattering event of ^4He on O sub-lattice is increased by a factor of 15 compared to standard Rutherford elastic backscattering [31]. However, the backscattering event of ^4He on U sub-lattice, proportional to Z^2 , remains around 7 times higher than for O sub-lattice. The damage evolution obtained by RBS-C analysis is more sensitive to the U than to the O sub-lattice disorder. As we clearly observed different evolution with Raman kinetics, the changes on Raman spectra seems to be more sensitivity to damage on the O sub-lattice in good agreement with the literature where the U1 and U3 bands are correlated with oxygen sub- or sur-stoichiometry, respectively [7,10, 32].

Conclusions

In situ Raman coupled with ion irradiation at low energy have been carried out on uranium dioxide. The results confirmed that polycrystalline samples were not amorphized by nuclear damage even for very high defect level (200 dpa). Quite similar maximum asymptotic value of the defect massif area and of T_{2g} band width was found for all the investigated projectiles. Only the shape evolution of defect

massif area change with the irradiation temperature. Indeed, the saturation is achieved at a smaller defect level for low temperature (-160°C) than at 25°C. The study of the damage kinetics evolution induced by ion irradiations shows a good match between voids nucleation and Raman spectra changes (massif of defects). On the contrary, the evolutions kinetics of dislocations and of damage fraction obtained by RBS-C are very different from the one observed in the current work. It should indicate that the defect massif increase is linked to the formation of point defect and defect cluster evolving in the void nucleation. Future work will aim at correlating the microstructural evolution by TEM and the Raman spectra change in uranium dioxide.

ACKNOWLEDGMENTS

The staffs of the JANNUS facilities at Saclay are sincerely acknowledged for their assistance during ion irradiations.

Reference

- [1] L. Desgranges, G. Guimbretière, P. Simon, C. Jegou, R. Caraballo, Nucl. Instrum. Meth. Phys. Res. Sect. B Beam Interact. with Mat. Atoms 315 (2013) 169.
- [2] J.-M. Costantini, A. Kahn-Harari, F. Beuneu, F. Couvreur, J. Appl. Phys., 99 (2006) 123501.
- [3] H.M. Anamul, M. Toulemonde, C. Jegou, S. Miro, Y. Serruys, S. Bouffard, S. Peugeot, Scien. Rep. 6 (2016) 30191.
- [4] J.M. Elorrieta, D. Manara, L.J. Bonales, J.F. Vigier, O. Dieste, M. Naji, R.C. Belin, V.G. Baonza, R.J.M. Konings, J. Cobos, J. Nucl. Mater. 495 (2017) 484.
- [5] Z. Talip, S. Peugeot, M. Magnin, M. Tribet, C. Valot, R. Vauchy, C. Jégou, J. Nucl. Mater. 499 (2018) 88.
- [6] P.R., Graves, App. Spect., 44 (1990) 1665.
- [7] G. Guimbretière, L. Desgranges, A. Canizares, G. Carlot, R. Caraballo, C. Jégou, F. Duval, N. Raimboux, M.R. Ammar, P. Simon, Appl. Phys. Lett. 100 (2012) 251914.
- [8] T. Livneh, J. Phys. Condens. Matter 20 (2008) 85202.
- [9] H. He, D. Shoesmith, Phys. Chem. Chem. Phys. 12 (2010) 8108.
- [10] L. Desgranges, G. Baldinozzi, P. Simon, G. Guimbretière, A. Canizares, J. Raman Spectrosc. 43 (2012) 455.
- [11] S. Miro, E. Bordas, L. Thomé, J.-M. Costantini, F. Leprêtre, P. Trocellier, Y. Serruys, L. Beck, D. Gosset, R. Verlet, J. Huguet-Garcia, M. Tupin, M. Belleil, J. Raman Spectrosc. 47 (2016) 476.
- [12] J. F. Ziegler, J. P. Biersack, U. Littmark, in The Stopping and Range of Ions in Solids, (Eds: J. F. Ziegler), Pergamon, New York, 1985, Vol. 1.
- [13] J. Soullard, J. Nucl. Mater. 135 (1985) 190.
- [14] V.G Keramidias, W.B. White, J. Chem. Phys. 59 (1973) 1561.
- [15] L. Desgranges, G. Guimbretière, P. Simon, F. Duval, A. Canizares, R. Omnee, C. Jégou, R. Caraballo, Nucl. Instrum. Methods Phys. Res. Sect. B Beam Interact. Mat. Atoms 327 (2014) 74.
- [16] R. Mohun, L. Desgranges, J. Léchelle, P. Simon, G. Guimbretière, A. Canizarès, F. Duval, C. Jegou, M. Magnin, N. Clavie, N. Dacheux, C. Valot, R. Vauchy, Nucl. Instrum. Methods Phys. Res. Sect. B Beam Interact. Mat. Atoms 374 (2016) 67.
- [17] J. Jagielski, L. Thomé, Appl. Phys. A, 105 (2009) 073513.
- [18] M. H. Brodsky and M. Cardona, J. Non-Cryst. Solids 31 (1978) 81.

- [19] X. Huang, F. Ninio, L.J. Brown, J. Appl. Phys., 77 (1995) 5910.
- [20] H. Matzke, A. Turos, Nucl. Instrum. Methods Phys. Res. Sect. B Beam Interact. Mat. Atoms 46 (1990) 117.
- [21] C. Onofri, C. Sabathier, H. Palanchar, G. Carlot, S. Miro, Y. Serruys, L. Desgranges, M. Legros, Nucl. Instrum. Methods Phys. Res. Sect. B Beam Interact. Mat. Atoms 374 (2016) 51.
- [22] L. F. He, M. Gupta, C. A. Yablinsky, J. Gan, M. A. Kirk, X. M. Bai, J. Pakarinen, T. R. Allen, J. Nucl. Mater. 443 (2013) 71.
- [23] C. Onofri, C. Sabathier, C. Baumier, C. Bachelet, H. Palanchar, M. Legros, J. Nucl. Mater. 482 (2016) 105.
- [24] L. F. He, J. Pakarinen, M. A. Kirk, J. Gan, A. T. Nelson, X. M. Bai, A. El-Azan, T. R. Allen, Nucl. Instrum. Methods Phys. Res. Sect. B Beam Interact. Mat. Atoms 330 (2014) 55.
- [25] C. Onofri, C. Sabathier, C. Baumier, C. Bachelet, H. Palanchar, B. Warot-Fonrose, M. Legros, Influence of exogenous xenon atoms on the evolution kinetics of extended defects in polycrystalline UO₂ using in situ TEM, will be submitted to JNM.
- [26] Y. Haddad, L. Delauche, A. Gentils, F. Garrido, Nucl. Instrum. Methods Phys. Res. Sect. B Beam Interact. Mat. Atoms in Press <https://doi.org/10.1016/j.nimb.2017.12.019>.
- [27] C. Sabathier, L. Vincent, P. Garcia, F. Garrido, G. Carlot, L. Thome, P. Martin, C. Valot Nucl. Instrum. Methods Phys. Res. Sect. B Beam Interact. Mat. Atoms 266 (2008) 3027.
- [28] C. Sabathier, G. Martin, A. Michel, G. Carlot, S. Maillard, C. Bachelet, F. Fortuna, O. Kaitasov, E. Oliviero, P. Garcia, Nucl. Instrum. Methods Phys. Res. Sect. B Beam Interact. Mat. Atoms 326 (2014) 247.
- [29] A. Michel, C. Sabathier, G. Carlot, O. Kaitasov, S. Bouffard, P. Garcia, C. Valot, Nucl. Instrum. Methods Phys. Res. Sect. B Beam Interact. Mat. Atoms 272 (2012) 218.
- [30] T. H. Nguyen, F. Garrido, A. Debelle, S. Mylonas, L. Nowicki, L. Thomé, J. Bourçois, J. Moeyaert, Nucl. Instrum. Methods Phys. Res. Sect. B Beam Interact. Mat. Atoms 326 (2014) 264.
- [31] H.S. Cheng, H. Shen, J. Tang, F. Yang, Nucl. Instrum. Methods Phys. Res. Sect. B Beam Interact. Mat. Atom 83 (1993) 449.
- [32] M. Razdan, D.W. Shoesmith, J. Electrochem. Soc. 161 (2013) H105.

TABLE

Table 1

	Energy (MeV)	Irradiation temperature (°C)	Flux (at.cm ⁻² .s ⁻¹)	R _p (nm)	Maximum dpa at 10 ¹⁵ at.cm ⁻²
I	0.9	25	1×10 ¹¹	150	7.5
Au	2	25	5×10 ¹¹	210	11.5
Kr	4	-160	5×10 ¹¹	420	3

Tab. 1: Irradiation conditions used during this study and simulated by SRIM software [12]. The projected range (R_p), the maximum displacement per atoms (dpa) have been simulated for a density of 10.74 g.cm⁻³, in full cascade mode with threshold displacement energies of 20 and 40 eV for the O and U sub-lattices, respectively [13].

FIGURE

Figure 1

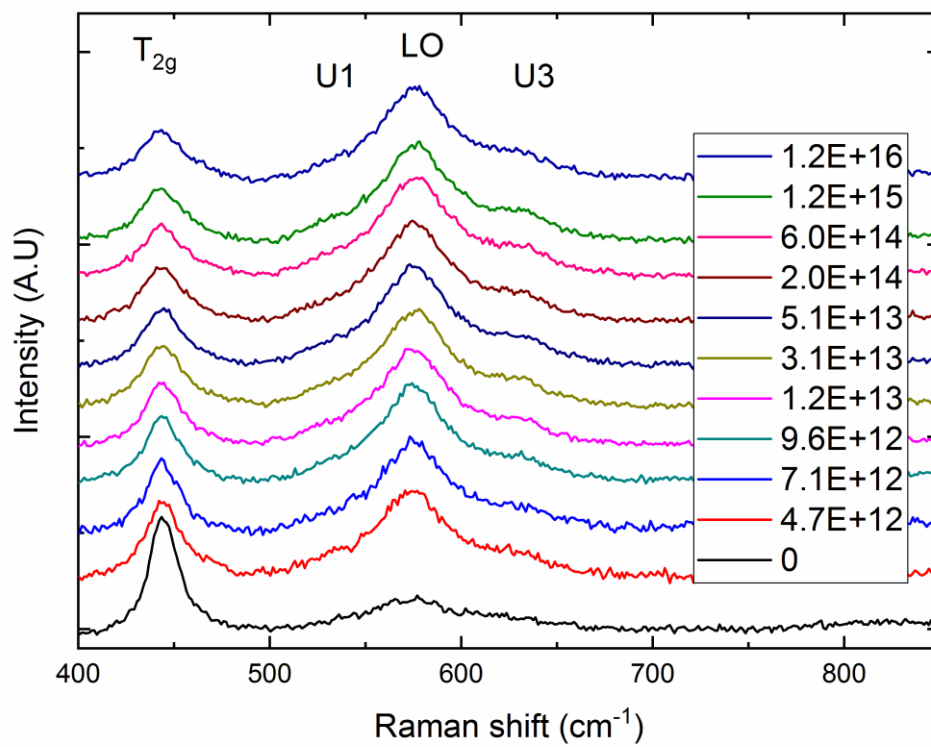


Fig. 1: In situ Raman spectra on UO_2 samples irradiated at 25°C with Au ions at an energy of 2 MeV.

Figure 2

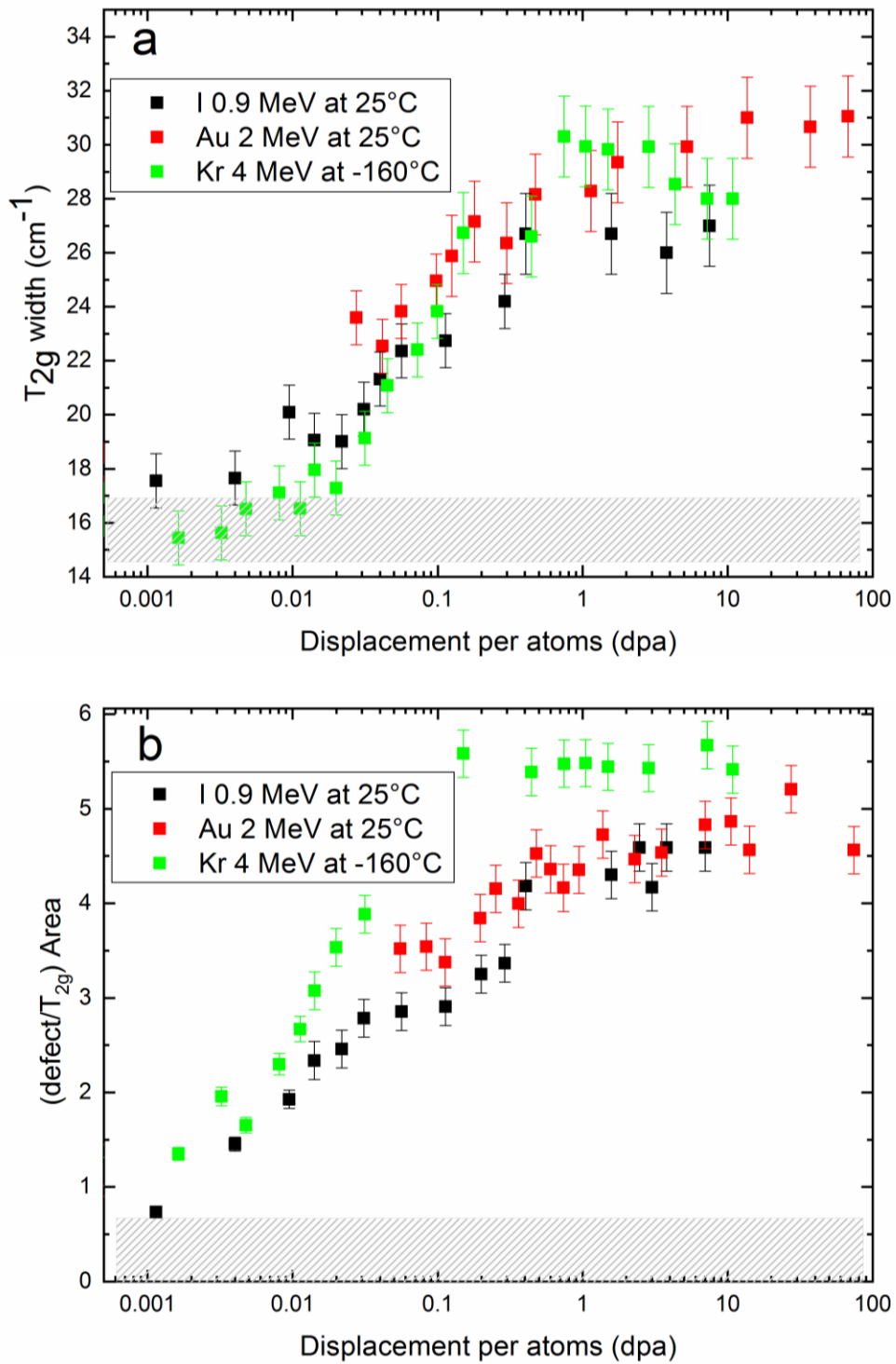


Fig. 2: (a) The T_{2g} width evolution and (b) the ratio between defect massif area and T_{2g} band area after irradiation with 0.9 MeV I ions and 2 MeV Au ions at 25°C. The hatched rectangles represent the reference T_{2g} width of virgin UO_2 before irradiation and the initial ratio.

Figure 3

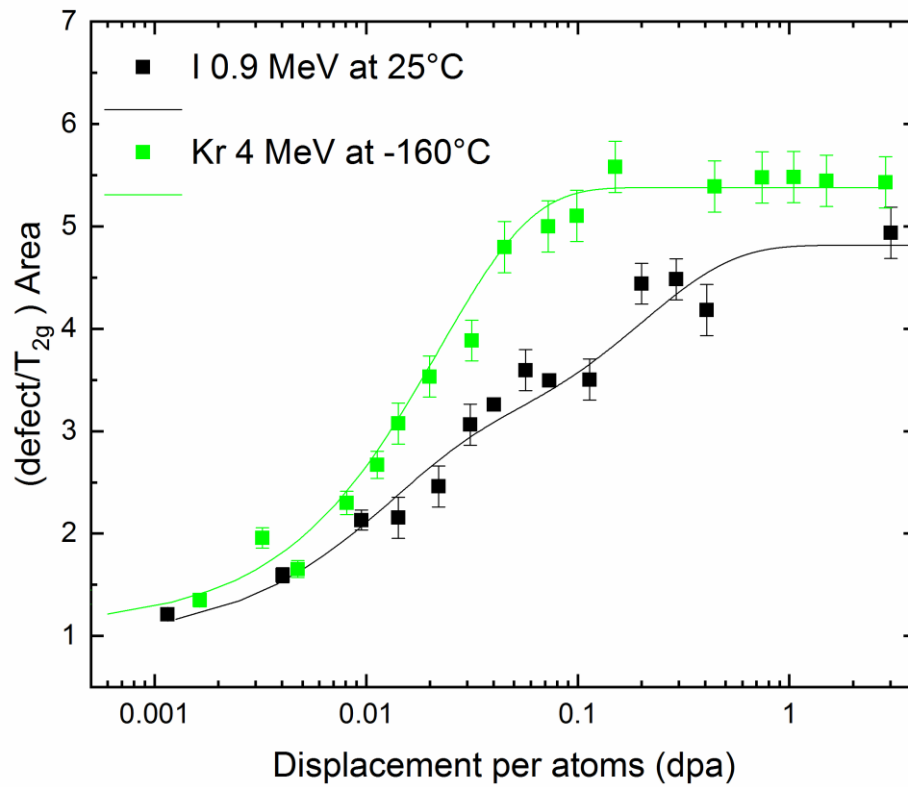


Fig. 3: The ratio between defect massif area and T_{2g} band area after irradiation with 0.9 MeV I ions and 4 MeV Kr ions at -180°C. The curves are fits of Raman data by the MSDA model [17].

Figure 4

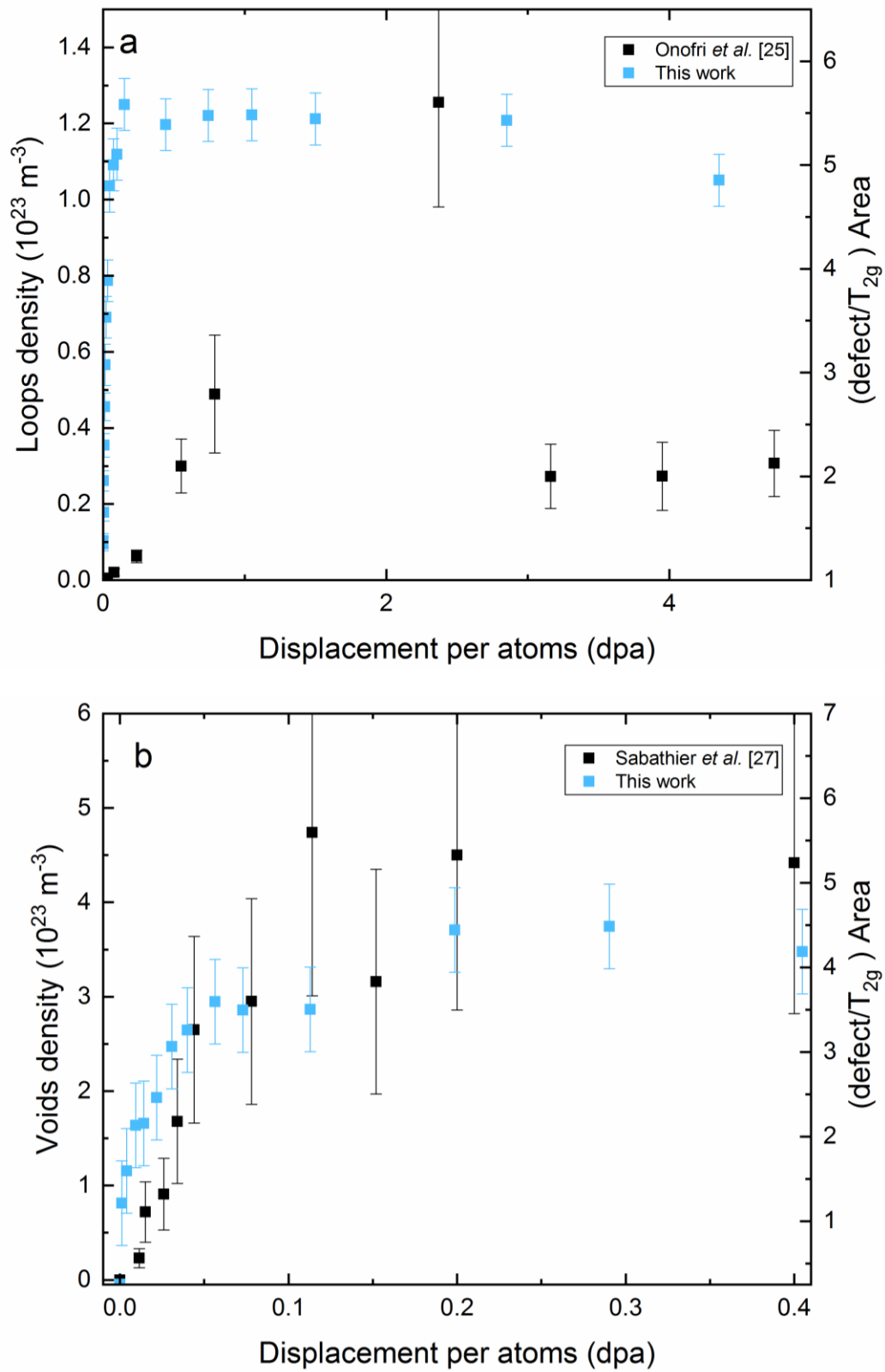


Fig. 4: a) Evolution of defect massif area obtained by Raman during 4 MeV Kr irradiation at -160°C compared to the loops density determined by TEM observations during 0.39 MeV Xe irradiation at -

180°C as function of the displacement per atoms [25]. b) Evolution of defect massif area obtained by Raman during 0.9 MeV I irradiation compared to the voids density determined by TEM observations during 4 MeV Au ions irradiation at 25°C as function of the displacement per atoms [27].

Figure 5

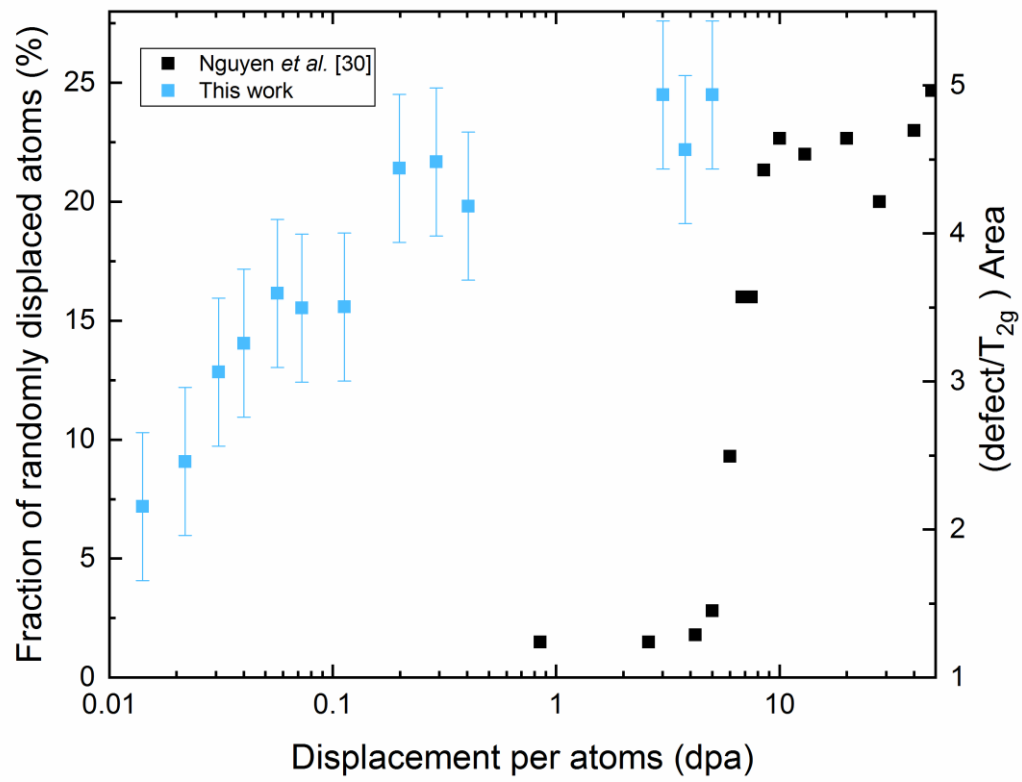


Fig. 5: Evolution of defect massif area obtained by Raman during 0.9 MeV I irradiation compared to fraction of randomly displaced atoms determined by RBS-C during 0.5 MeV La ions irradiation as function of the displacement per atoms [30].